

Supporting Information for the manuscript

## Enhanced CO<sub>2</sub> Sorption and Selectivity by Functionalization of a NbO-type Metal-Organic Framework with Polarized Benzothiadiazole Moieties

Chengling Song,<sup>a</sup> Yabing He,<sup>a\*</sup> Bin Li,<sup>b</sup> Yajing Ling,<sup>a</sup> Hailong Wang,<sup>b</sup> Yunlong Feng,<sup>a</sup>  
Rajamani Krishna,<sup>c</sup> Banglin Chen<sup>b\*</sup>

<sup>a</sup> College of Chemistry and Life Sciences, Zhejiang Normal University, Jinhua 321004, China. E-mail: heyabing@zjnu.cn.

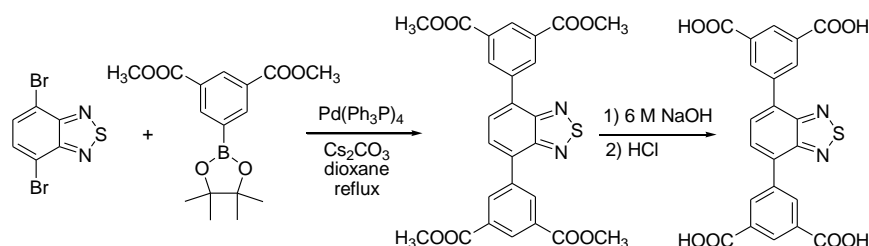
<sup>b</sup> Department of Chemistry, University of Texas at San Antonio, One UTSA Circle, San Antonio, Texas 78249-0698, USA. E-mail: banglin.chen@utsa.edu; Fax: +1-210-458-7428

<sup>c</sup> Van't Hoff Institute for Molecular Sciences, University of Amsterdam Science Park 904, 1098 XH Amsterdam (The Netherlands)

### General remarks

All starting materials and reagents for synthesis were commercially available and used as received. The <sup>1</sup>H NMR and <sup>13</sup>C NMR spectra were recorded on a Bruke Avance 600 spectrometer. Fourier transform infrared (FTIR) spectrum was recorded using a Nicolet 5DX FT-IR spectrometer. Thermogravimetric analyses (TGA) were carried out using a Netzsch STA 449C thermal analyzer with a heating rate of 5 °C min<sup>-1</sup> in a flowing nitrogen atmosphere (10 mL min<sup>-1</sup>). Powder X-ray diffraction (PXRD) patterns were recorded on a Philips PW3040/60 automated powder diffractometer, using Cu-K<sub>α</sub> radiation ( $\lambda = 1.542 \text{ \AA}$ ) with a  $2\theta$  range of 5–45°. The elemental analyses were performed with Perkin–Elmer 240 CHN analyzers. The crystal data were collected on a Bruker APEX II diffractometer equipped with a graphite-monochromatized Mo-K<sub>α</sub> radiation ( $\lambda = 0.71073 \text{ \AA}$ ) at 296(2) K. Data intensity was corrected by Lorentz-polarization factors and empirical absorption. The structures were solved by direct methods and expanded with difference Fourier techniques. All calculations were performed using SHELXS-97 and SHELXL-97 program packages. A Micromeritics ASAP 2020 surface area analyzer was used to measure gas adsorption isotherms. To have a guest-free framework, the fresh sample was guest-exchanged with dry acetone at least 10 times, filtered and vacuumed at 373 K until the outgas rate was 6  $\mu\text{mHg min}^{-1}$  prior to measurements. A sample of 113.7 mg was used for the sorption measurements and was maintained at 77 K with liquid nitrogen, and at 273 K with an ice–water bath. As the center-controlled air conditioner was set up at 23 °C, a water bath was used for adsorption isotherms at 296 K.

## Synthesis and characterization of the organic building block (H<sub>4</sub>L)



**Scheme 1** Synthetic route to the organic linker used to construct **ZJNU-40**.

To a mixture of 4,7-dibromobenzo[c][1,2,5]thiadiazole (0.50 g, 1.70 mmol), dimethyl 5-(pinacolboron)isophthalate (1.20 g, 3.74 mmol), Cs<sub>2</sub>CO<sub>3</sub> (1.66 g, 5.10 mmol) and Pd(PPh<sub>3</sub>)<sub>4</sub> (0.10 g, 0.09 mmol) were added dry dioxane (40 mL). The resulting mixture was stirred under reflux under a nitrogen atmosphere for 72 hr. After removal of the solvents, CH<sub>2</sub>Cl<sub>2</sub> (100 mL) and H<sub>2</sub>O (100 mL) were added. The mixture was filtered, washed with water and CH<sub>2</sub>Cl<sub>2</sub> sequentially, and dried under vacuum. The solid was hydrolyzed with 6 M NaOH, filtered and acidified with concentrated HCl to afford the target compound as a yellow solid in 66% yield (0.52 g, 1.12 mmol). <sup>1</sup>H NMR (DMSO-*d*<sub>6</sub>, 600.1 MHz)  $\delta$  (ppm): 13.50 (s, br, 4H), 8.81 (d, *J* = 1.8 Hz, 4H), 8.57 (t, *J* = 1.8 Hz, 2H), 8.15 (s, 2H); <sup>13</sup>C NMR (DMSO-*d*<sub>6</sub>, 150.9 MHz)  $\delta$  (ppm): 166.41, 152.95, 137.32, 133.66, 131.67, 130.97, 129.63, 128.89; selected FTIR (KBr, cm<sup>-1</sup>): 1732, 1709, 1601, 1554, 1441, 1404, 1304, 1271, 1215, 1161, 1124, 916, 895, 854, 802, 756, 708, 685, 667, 548, 519.

## Synthesis and characterization of ZJNU-40

A mixture of the organic linker H<sub>4</sub>L (5.0 mg, 10.7  $\mu$ mol) and Cu(NO<sub>3</sub>)<sub>2</sub>·3H<sub>2</sub>O (15.0 mg, 62.1  $\mu$ mol) was dissolved into a mixed solvent of *N,N*-diethylformamide (DEF) and H<sub>2</sub>O (1.5 mL / 0.08 mL) in a screw-capped vial (20 mL). 50  $\mu$ L of 6 M HCl were then added. The vial was capped and heated at 353 K for 96 h. Blue rhombic crystals were obtained in 67% yield. **ZJNU-40** can be best formulated as [Cu<sub>2</sub>L(H<sub>2</sub>O)<sub>2</sub>]<sub>2</sub>·4DEF·6H<sub>2</sub>O on the basis of single-crystal X-ray diffraction structure determination, TGA and microanalysis. Selected FTIR (KBr, cm<sup>-1</sup>): 1660, 1591, 1568, 1495, 1444, 1417, 1381, 1093, 1049, 879, 777, 754, 729; TGA data for loss of 4DEF+8H<sub>2</sub>O, calcd: 46.6%, found: 48.0%; anal. for C<sub>42</sub>H<sub>64</sub>Cu<sub>2</sub>N<sub>6</sub>O<sub>18</sub>S, calcd: C, 45.85%, H, 5.86%, N, 7.64%; found: C, 48.59%, H, 5.90%, N, 7.55%.

## Fitting of pure-component isotherms

The measured experimental data on *excess* loadings,  $q^{\text{excess}}$ , of the pure components CO<sub>2</sub>, CH<sub>4</sub>, and N<sub>2</sub> in **ZJNU-40a** and **NOTT-101**, were first converted to absolute loadings,  $q$ , using

$$q = q^{excess} + \frac{pV_{pore}}{ZRT} \quad (1)$$

where  $Z$  is the compressibility factor. The Peng-Robinson equation of state was used to estimate  $Z$ . The accessible pore volume for **ZJNU-40a** and **NOTT-101** are  $0.8806 \text{ cm}^3 \text{ g}^{-1}$  and  $1.0485 \text{ cm}^3 \text{ g}^{-1}$ , respectively.

The absolute component loadings were fitted with the Langmuir model

$$q = q_{sat} \frac{bp}{1 + bp} \quad (2)$$

with  $T$ -dependent parameter  $b$

$$b = b_0 \exp\left(\frac{E}{RT}\right) \quad (3)$$

The Langmuir parameters for adsorption of  $\text{CO}_2$  are provided in *Tables S3*, and *S4* for **ZJNU-40a** and **NOTT-101**.

*Figure S6* provides a comparison of the experimental isotherm data for (a)  $\text{CO}_2$ , (b)  $\text{CH}_4$ , and (c)  $\text{N}_2$  in **ZJNU-40a** with the isotherm fits. *Figure S7* provides a comparison of the experimental isotherm data for (a)  $\text{CO}_2$ , (b)  $\text{CH}_4$ , and (c)  $\text{N}_2$  in **NOTT-101** with the isotherm fits. For all guest/host combinations, the isotherm fits are excellent.

## Isosteric heat of adsorption

The isosteric heat of adsorption,  $Q_{st}$ , defined as

$$Q_{st} = RT^2 \left( \frac{\partial \ln p}{\partial T} \right)_q \quad (4)$$

was determined using the Clausius-Clapeyron equation by fitting the adsorption isotherms taken at 273 and 296 K to a Langmuir expression. The values of  $Q_{st}$  for  $\text{CO}_2$ ,  $\text{CH}_4$ , and  $\text{N}_2$  in **ZJNU-40a**, and **NOTT-101** are shown in *Figure S17*.

## IAST calculations of adsorption selectivities and uptake capacities

The selectivity of preferential adsorption of component  $1$  over component  $2$  in a mixture containing  $1$  and  $2$ , perhaps in the presence of other components too, can be formally defined as

$$S_{ads} = \frac{q_1/q_2}{p_1/p_2} \quad (5)$$

In equation (5),  $q_1$  and  $q_2$  are the absolute component loadings of the adsorbed phase in the mixture. These component loadings are also termed the uptake capacities. We calculate the values of  $q_1$  and  $q_2$  using the Ideal Adsorbed Solution Theory (IAST) of Myers and Prausnitz.<sup>1</sup>

*Figures S8a* and *S8b* present the values of the adsorption selectivity for (a) 50/50

CO<sub>2</sub>/CH<sub>4</sub>, and (b) 5/95 CO<sub>2</sub>/CH<sub>4</sub> gas mixtures maintained at isothermal conditions at 296 K in **ZJNU-40a**, and **NOTT-101**. We note that **ZJNU-40a** has higher selectivity towards CO<sub>2</sub> for both mixture compositions.

**ZJNU-40a** has a higher selectivity towards CO<sub>2</sub> for adsorption from 15/85 CO<sub>2</sub>/N<sub>2</sub> gas mixtures; see *Figure S8c*.

Besides the adsorption selectivities, the separation performance is also dictated by uptake capacities. *Figures S9a, S9b, and S9c* present IAST calculations for uptake of CO<sub>2</sub> from (a) 50/50 CO<sub>2</sub>/CH<sub>4</sub>, (b) 5/95 CO<sub>2</sub>/CH<sub>4</sub>, and (c) 15/85 CO<sub>2</sub>/N<sub>2</sub> gas mixtures maintained at isothermal conditions at 296 K in **ZJNU-40a**, and **NOTT-101**. **ZJNU-40a** has higher uptake of CO<sub>2</sub> in all three cases.

The combination of higher selectivity and higher uptake of CO<sub>2</sub> is most desirable and leads to enhanced separations in fixed beds.

## Transient breakthroughs in fixed bed adsorbers

The performance of industrial fixed bed adsorbers is dictated by a combination of *adsorption selectivity* and *uptake capacity*. For a proper comparison of various MOFs, we perform transient breakthrough simulations using the simulation methodology described in the literature.<sup>2-6</sup> For the breakthrough simulations, the following parameter values were used: length of packed bed,  $L = 0.3$  m; voidage of packed bed,  $\varepsilon = 0.4$ ; superficial gas velocity at inlet,  $u = 0.04$  m s<sup>-1</sup>; see schematic in *Figure S10*.

The transient breakthrough simulation results are presented in terms of a dimensionless time,  $\tau$ , defined by dividing the actual time,  $t$ , by the characteristic time,  $\frac{L\varepsilon}{u}$ .

*Figure S11* compares 50/50 CO<sub>2</sub>/CH<sub>4</sub> mixture breakthrough characteristics as a function of the dimensionless time in an adsorber packed with **ZJNU-40a** and **NOTT-101**. For both materials the sequence of breakthroughs is CH<sub>4</sub>, and CO<sub>2</sub> that is dictated by the adsorption strengths; the more strongly adsorbing CO<sub>2</sub> elutes last in the sequence. The breakthrough of CO<sub>2</sub> occurs at a later time with **ZJNU-40a** and this material has the better separation performance. The reason for the improved separation can be traced to two separate factors: (a) higher CO<sub>2</sub> uptake capacity of **ZJNU-40a**, and (b) higher CO<sub>2</sub>/CH<sub>4</sub> adsorption selectivities.

In natural gas purification processes, the primary objective is to produce CH<sub>4</sub> with a specified purity level, which is typically 500 ppm CO<sub>2</sub>, *i.e.* 0.05 mole % CO<sub>2</sub>. Let us compare the productivities of pure CH<sub>4</sub> that fulfills the specified impurity level for CO<sub>2</sub>. *Figure S12* presents a comparison of the % CH<sub>4</sub> exiting the adsorber packed with **ZJNU-40a**, and **NOTT-101**. During the time interval  $\Delta\tau$ , 99.95%+ pure CH<sub>4</sub> can be produced. These amounts can be determined from a material balance on the fixed bed adsorber; the productivities are 2.84 mol *per* kg of **ZJNU-40a**, and 1.78 mol *per* kg of **NOTT-101**. This implies that **ZJNU-40a** has a 50% higher productivity than **NOTT-101**.

Let us consider separations of 5/95 CO<sub>2</sub>/CH<sub>4</sub> mixtures. *Figure S13* compares 5/95 CO<sub>2</sub>/CH<sub>4</sub> mixture breakthrough characteristics of **ZJNU-40a** and **NOTT-101**. *Figure*

S14 presents a comparison of the % CH<sub>4</sub> exiting the adsorber packed with **ZJNU-40a**, and **NOTT-101**. From a material balance on the fixed bed adsorber; the productivities are 5.80 mol *per* kg of **ZJNU-40a**, and 3.62 mol *per* kg of **NOTT-101**. These productivity values are higher than the corresponding ones for 50/50 mixtures because of the lower amount of CO<sub>2</sub> that needs to be captured. For 5/95 CO<sub>2</sub>/CH<sub>4</sub> mixtures, **ZJNU-40a** has a 60% higher productivity than **NOTT-101**.

Let us now compare separations of 15/85 CO<sub>2</sub>/N<sub>2</sub> gas mixtures that is relevant for CO<sub>2</sub> capture from flue gases. *Figure S15* presents the 15/85 CO<sub>2</sub>/N<sub>2</sub> mixture breakthrough characteristics as a function of the dimensionless time in an adsorber packed with **ZJNU-40a**, and **NOTT-101** at a total pressure of 100 kPa. N<sub>2</sub> with a purity of 99.95% can be produced during the time interval  $\Delta\tau$ , as indicated in *Figure S16*. The productivity can be determined to be 3.29 mol *per* kg of **ZJNU-40a**, and 2.08 mol *per* kg of **NOTT-101**.

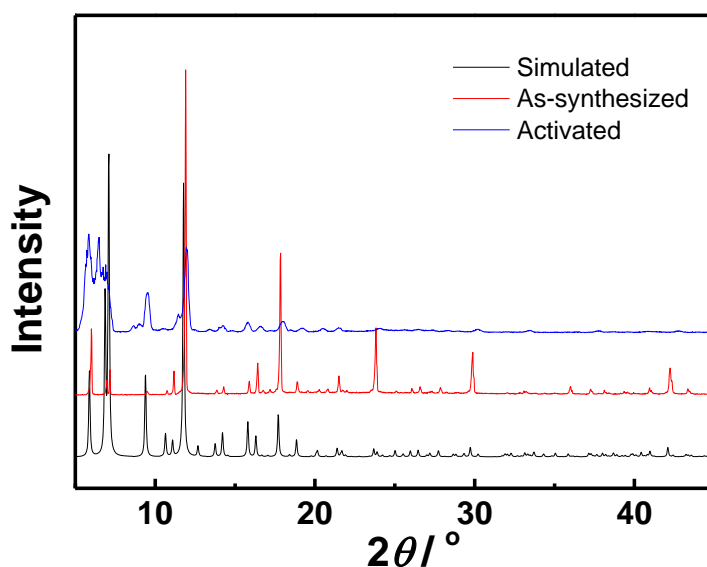


*Fig. S1* PXRD patterns of the as-synthesized **ZJNU-40** (red) and the activated **ZJNU-40a** (blue), along with the one simulated from the cif file (black).

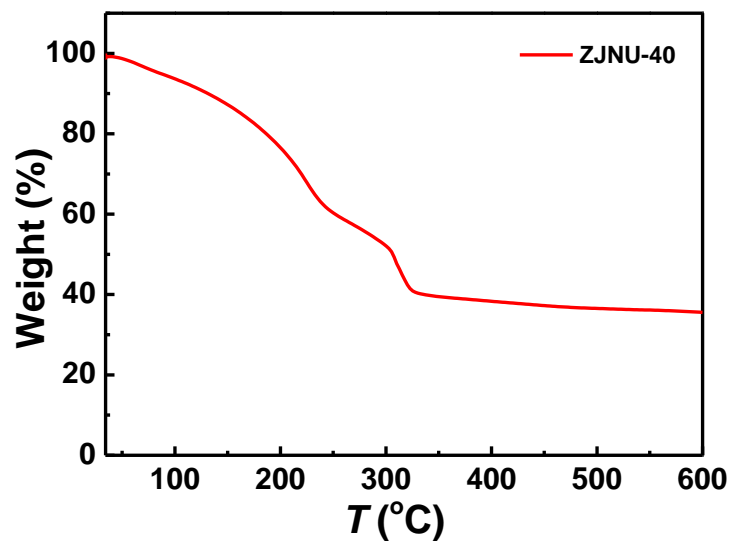


Fig. S2 TGA curve of the as-synthesized ZJNU-40 under a nitrogen atmosphere.

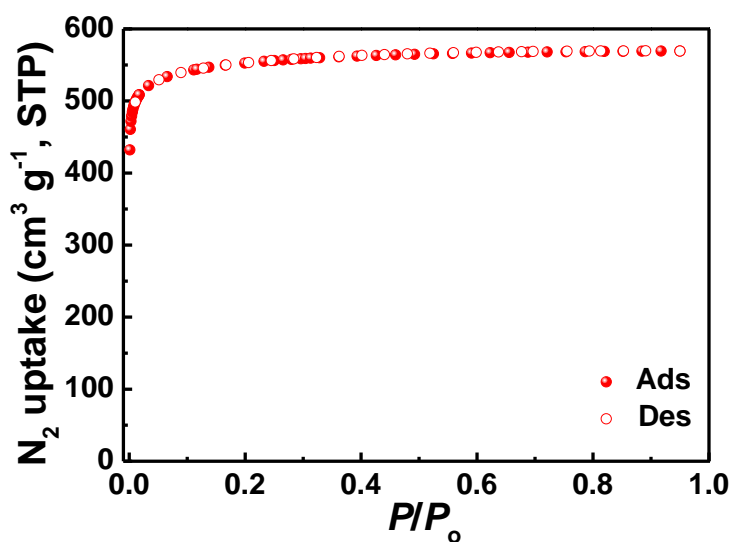


Fig. S3 N<sub>2</sub> sorption isotherm of ZJNU-40a at 77 K. The solid and open symbols represent adsorption and desorption, respectively.

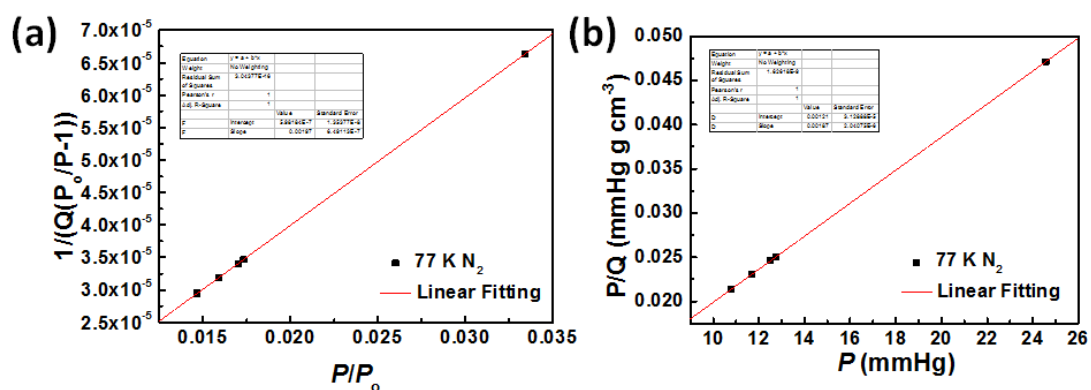
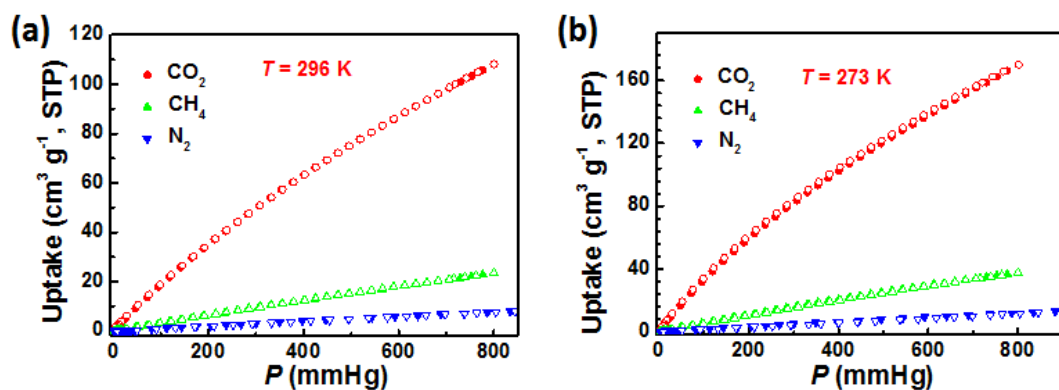


Fig. S4 BET and Langmuir analysis from N<sub>2</sub> adsorption isotherm at 77 K.

$$S_{\text{BET}} = 1/(0.00197 + 5.98184 \times 10^{-7})/22414 \times 6.023 \times 10^{23} \times 0.162 \times 10^{-18} = 2209 \text{ m}^2 \text{ g}^{-1}$$

$$S_{\text{Langmuir}} = (1/0.00187)/22414 \times 6.023 \times 10^{23} \times 0.162 \times 10^{-18} = 2328 \text{ m}^2 \text{ g}^{-1}$$



**Fig. S5** CO<sub>2</sub>, CH<sub>4</sub> and N<sub>2</sub> sorption isotherms of **ZJNU-40a** at 296 K (a), and 273 K (b). The solid and open symbols represent adsorption and desorption, respectively.

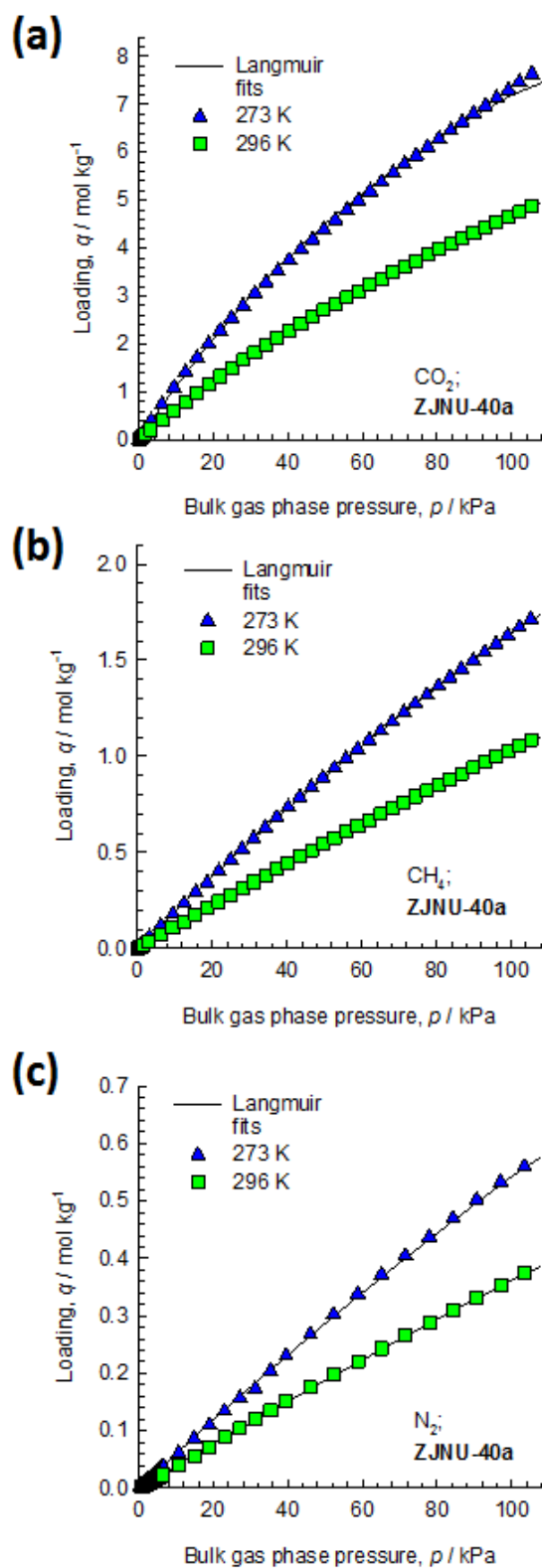


**Fig. S6** Comparison of the pure-component isotherm data for (a) CO<sub>2</sub>, (b) CH<sub>4</sub>, and (c) N<sub>2</sub> in **ZJNU-40a** with the fitted isotherms (shown by continuous solid lines) at 273 K, and 296 K.



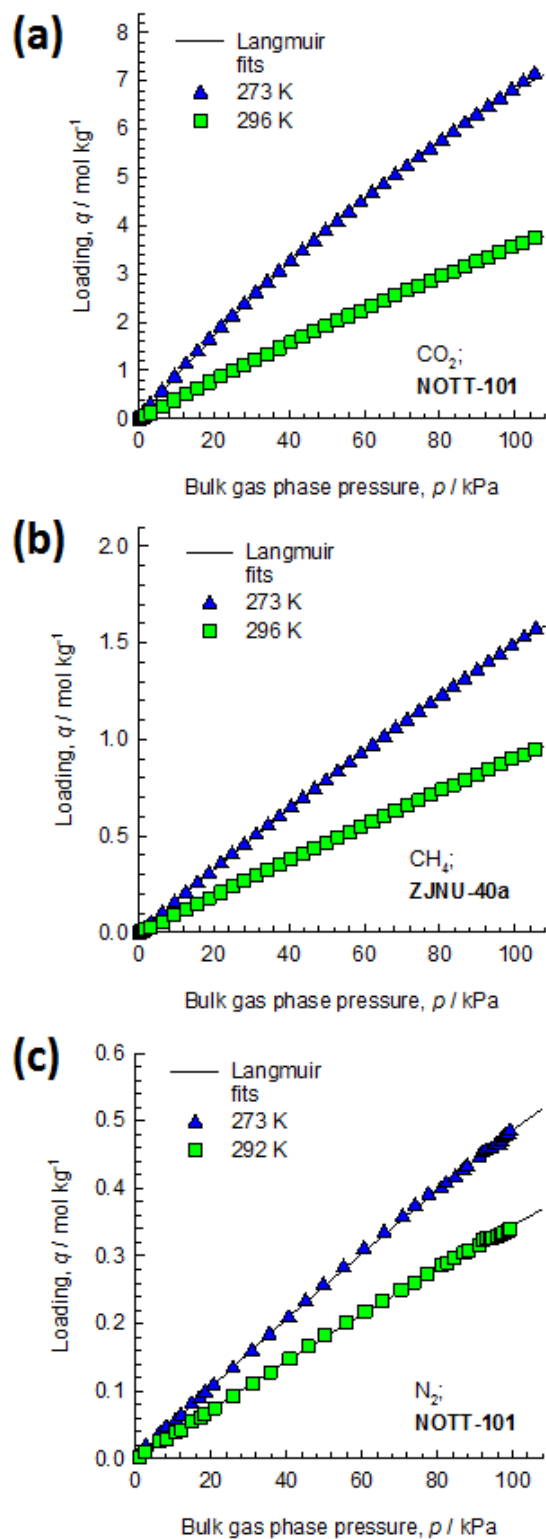


**Fig. S7** Comparison of the pure-component isotherm data for (a)  $\text{CO}_2$ , (b)  $\text{CH}_4$ , and (c)  $\text{N}_2$  in NOTT-101 with the fitted isotherms (shown by continuous solid lines).

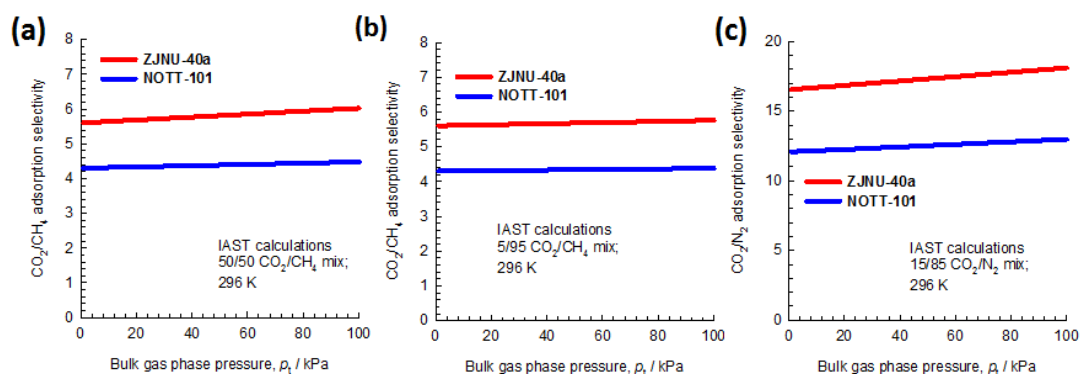


**Fig. S8** Calculations using Ideal Adsorbed Solution Theory (IAST) of Myers and Prausnitz<sup>1</sup> for adsorption selectivities for (a) 50/50 CO<sub>2</sub>/CH<sub>4</sub>, (b) 5/95 CO<sub>2</sub>/CH<sub>4</sub>, and (c) 15/85 CO<sub>2</sub>/N<sub>2</sub> gas mixtures maintained at isothermal conditions at 296 K in ZJNU-40a, and NOTT-101.

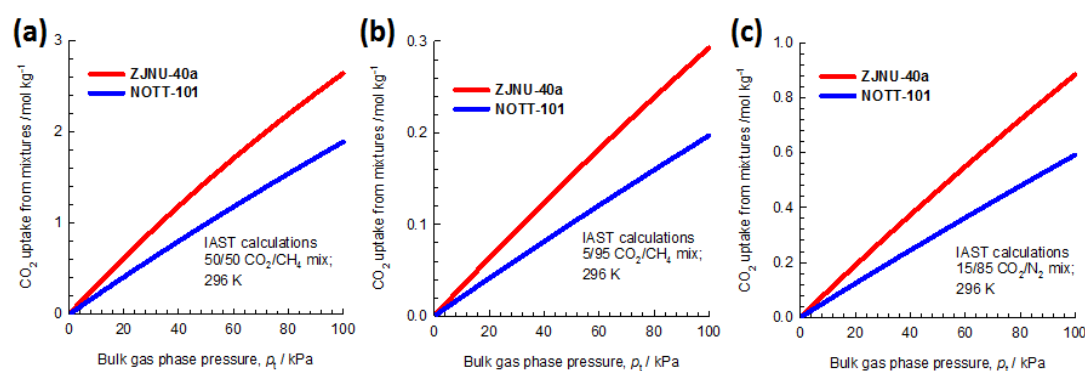


**Fig. S9** Calculations using Ideal Adsorbed Solution Theory (IAST) of Myers and Prausnitz<sup>1</sup> for uptake of CO<sub>2</sub> from (a) 50/50 CO<sub>2</sub>/CH<sub>4</sub>, (b) 5/95 CO<sub>2</sub>/CH<sub>4</sub>, and (c) 15/85 CO<sub>2</sub>/N<sub>2</sub> gas mixtures maintained at isothermal conditions at 296 K in ZJNU-40a, and NOTT-101.

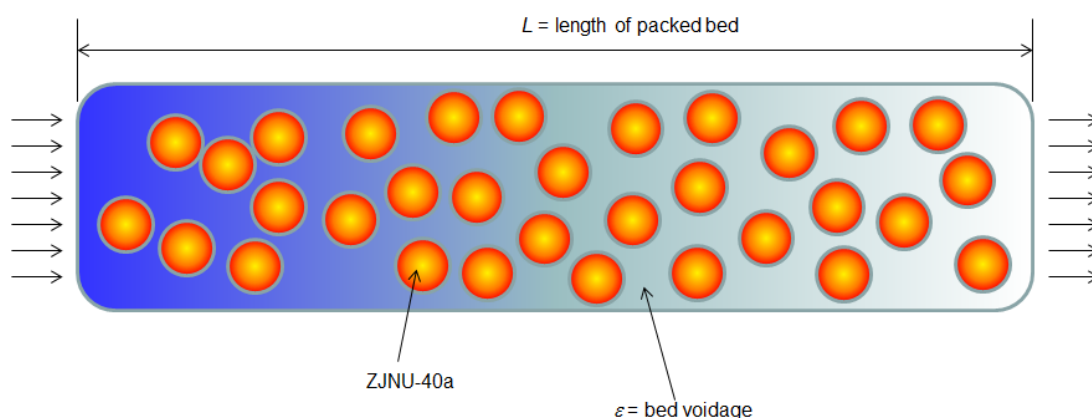


**Fig. S10** Schematic of the breakthrough apparatus. The tube length  $L = 0.3$  m. The apparatus is operated at 296 K, and at a total gas pressure of 200 kPa or 100 kPa. The bed porosity,  $\varepsilon = 0.4$ . The interstitial gas velocity,  $v = 0.04$  m s<sup>-1</sup>.

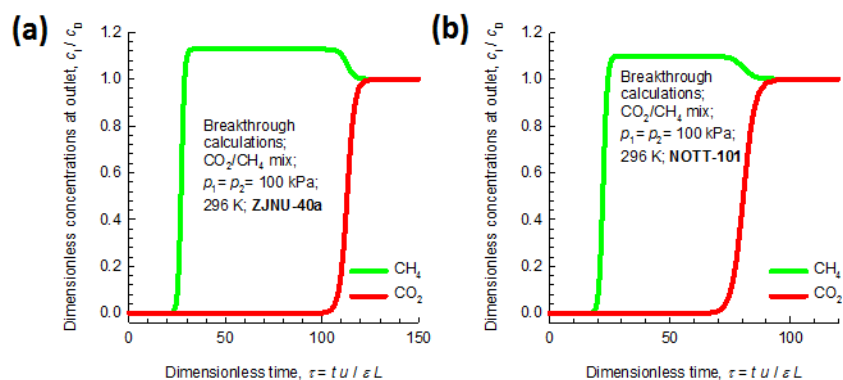


**Fig. S11** 50/50 CO<sub>2</sub>/CH<sub>4</sub> mixture breakthrough characteristics as a function of the dimensionless time in an adsorber packed with (a) **ZJNU-40a**, and (b) **NOTT-101** and maintained at isothermal conditions at 296 K. In these calculations, the total pressure is maintained at 200 kPa.

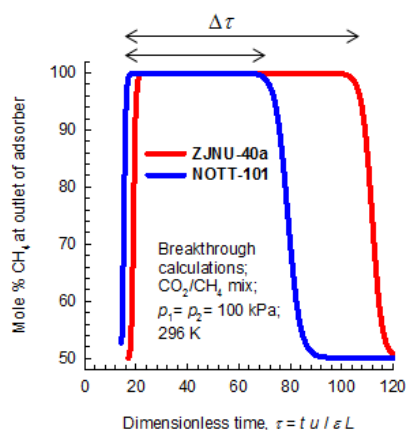


**Fig. S12** Comparison of the %CH<sub>4</sub> exiting the adsorber packed with **ZJNU-40a**, and **NOTT-101** fed with 50/50 CO<sub>2</sub>/CH<sub>4</sub> gas mixtures at 200 kPa total pressure and 296 K.

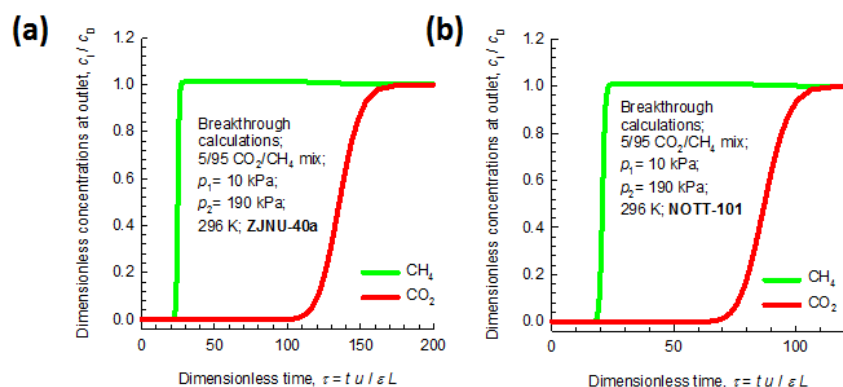


**Fig. S13** 5/95 CO<sub>2</sub>/CH<sub>4</sub> mixture breakthrough characteristics as a function of the dimensionless time in an adsorber packed with (a) **ZJNU-40a**, and (b) **NOTT-101** and maintained at isothermal conditions at 296 K. In these calculations, the total pressure is maintained at 200 kPa.

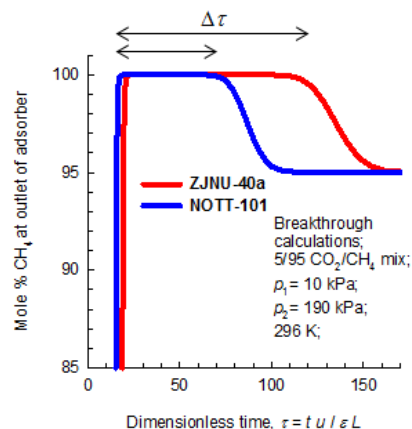


**Fig. S14** Comparison of the %CH<sub>4</sub> exiting the adsorber packed with **ZJNU-40a**, and **NOTT-101** fed with 5/95 CO<sub>2</sub>/CH<sub>4</sub> gas mixtures at 200 kPa total pressure and 296 K.

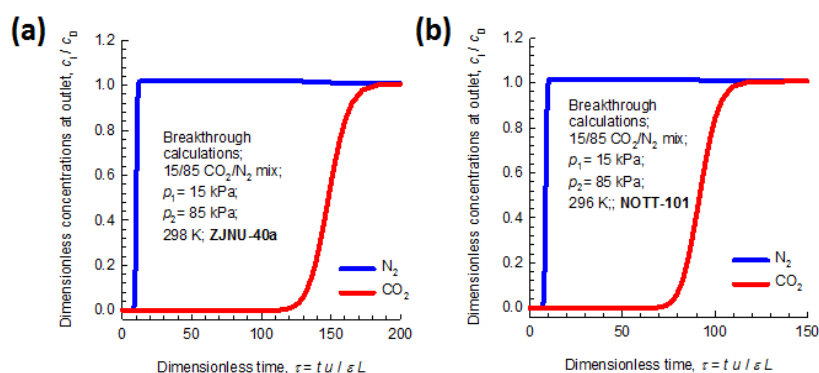


**Fig. S15** 15/85 CO<sub>2</sub>/N<sub>2</sub> mixture breakthrough characteristics as a function of the dimensionless time in an adsorber packed with (a) **ZJNU-40a**, and (b) **NOTT-101** and maintained at isothermal conditions at 296 K. In these calculations, the total pressure is maintained at 100 kPa.

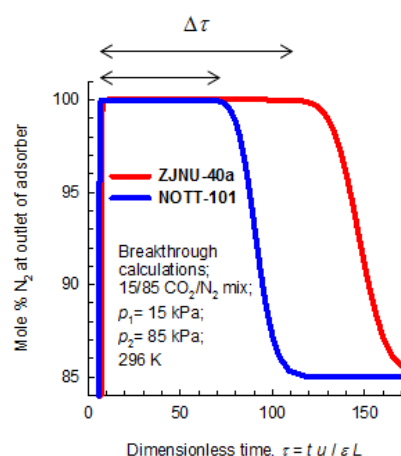


**Fig. S16** Comparison of the % N<sub>2</sub> exiting the adsorber packed with **ZJNU-40a**, and **NOTT-101** fed with 15/85 CO<sub>2</sub>/N<sub>2</sub> gas mixtures at 100 kPa total pressure and 296 K.

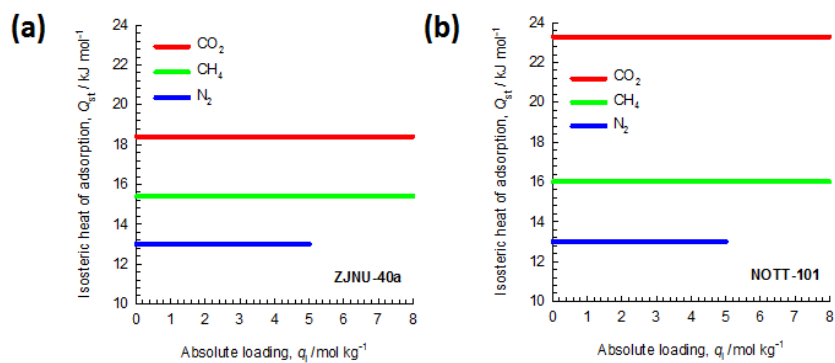


**Fig. S17** Isothermic heats of adsorption of  $\text{CO}_2$ ,  $\text{CH}_4$ , and  $\text{N}_2$  in **ZJNU-40a** (a) and **NOTT-101** (b).

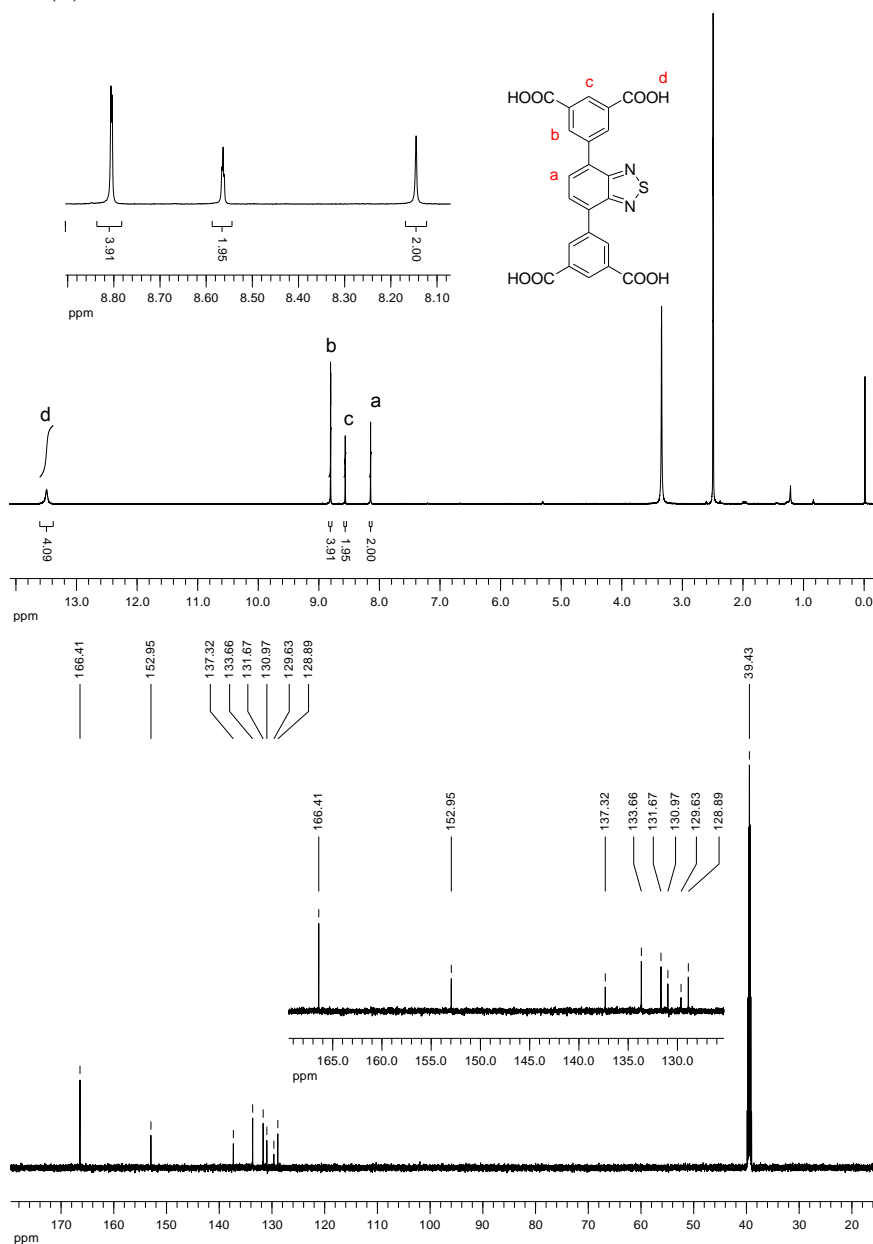


**Fig. S18**  $^1\text{H}$  NMR (DMSO- $d_6$ , 600.1 MHz) and  $^{13}\text{C}$  NMR (DMSO- $d_6$ , 150.9 MHz) spectra of the organic linker  $\text{H}_4\text{L}$ .

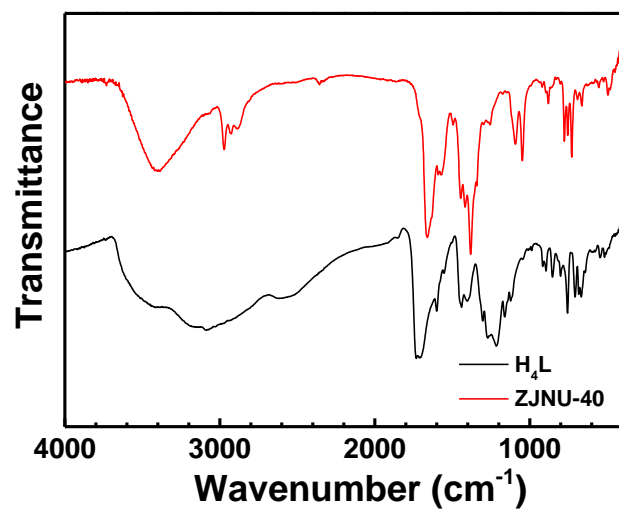


**Fig. S19** FTIR spectra of the organic linker H<sub>4</sub>L (black) and as-synthesized **ZJNU-40** (red).

**Table S1.** Crystal data and structure refinement for **ZJNU-40**.

Empirical formula	C <sub>66</sub> H <sub>24</sub> Cu <sub>6</sub> N <sub>6</sub> O <sub>32</sub> S <sub>3</sub>
Formula weight	1890.42
Temperature (K)	296(2)
Wavelength (Å)	0.71073
Crystal system, space group	Trigonal, <i>R</i> -3m
Unit cell dimensions	<i>a</i> = 18.819(4) Å <i>b</i> = 18.819(4) Å <i>c</i> = 38.603(15) Å <i>α</i> = 90° <i>β</i> = 90° <i>γ</i> = 120°
Volume (Å <sup>3</sup> )	11840(6)
Z, Calculated density (g cm <sup>-3</sup> )	3, 0.795
Absorption coefficient (mm <sup>-1</sup> )	0.877
<i>F</i> (000)	2820
Crystal size (mm)	0.2 × 0.18 × 0.12
<i>θ</i> range for data collection (°)	3.27 to 27.56
Limiting indices	-24 ≤ <i>h</i> ≤ 24 -24 ≤ <i>k</i> ≤ 24 -50 ≤ <i>l</i> ≤ 50
Reflections collected / unique	42313 / 3293 ( <i>R</i> <sub>int</sub> = 0.0339)
Completeness to <i>θ</i> = 27.56	99.0%
Absorption correction	Semi-empirical from equivalents
Max. and min. transmission	0.900 and 0.839
Refinement method	Full-matrix least-squares on <i>F</i> <sup>2</sup>
Data / restraints / parameters	3293 / 1 / 124
Goodness-of-fit on <i>F</i> <sup>2</sup>	1.132
Final R indices [ <i>I</i> > 2σ( <i>I</i> )]	<i>R</i> <sub>1</sub> = 0.0544, <i>wR</i> <sub>2</sub> = 0.1823
R indices (all data)	<i>R</i> <sub>1</sub> = 0.0612, <i>wR</i> <sub>2</sub> = 0.1910
Largest diff. peak and hole (e.Å <sup>-3</sup> )	1.137 and -0.335
CCDC	1014276

**Table S2.** BET surface area, pore volume and CO<sub>2</sub> adsorption of the reported Cu-based NbO-type MOFs.

MOFs	BET <sup>a</sup> (m <sup>2</sup> g <sup>-1</sup> )	V <sub>p</sub> <sup>b</sup> (cm <sup>3</sup> g <sup>-1</sup> )	CO <sub>2</sub> uptake under 1 atm at RT (cm <sup>3</sup> g <sup>-1</sup> )	Q <sub>st</sub> <sup>c</sup> (kJ mol <sup>-1</sup> )	Selectivity <sup>d</sup> CO <sub>2</sub> /CH <sub>4</sub>	Selectivity <sup>d</sup> CO <sub>2</sub> /N <sub>2</sub>	Ref.
<b>ZJNU-40</b>	<b>2209</b>	<b>0.8806</b>	<b>108</b>	<b>18.4</b>	<b>6.6</b>	<b>22.9</b>	<b>This work</b>
HNUST-1	1400	0.571	93	31.2			7
MOF-505	1547		73				8
UTSA-40	1630	0.65	73	24.0	5.6		9
Cu <sub>2</sub> dbip	1773	0.81	122	28.1		21.1	10
Cu <sub>2</sub> ebtc	1852	1.008					11
ZJU-25	2124	1.183	83		5.5		12
SNU-50	2300	1.08	80	25.8			13
HNUST-2	2366	0.97		23.5	4.9	22.9	14
NJU-Bai14	2384		100	24.5			15
HNUST-3	2421	0.99	84.5	24.8	7.9	26.1	16
NOTT-125a	2447	1.1	93		4.8	16	17
NU-135	2530	1.02	79	25.5	4	14.5	18
NOTT-101	2805	1.080	83	23.3	4.6		3
ZJU-5	2823	1.074	85				19
Cu <sub>2</sub> abtc	(2850) <sup>e</sup>	1.00					20
NJU-Bai12	3038	1.135		23.5	5.0	24.6	21
NOTT-102	3342	1.268	72 <sup>f</sup>		4.84		3

<sup>a</sup> BET surface area; <sup>b</sup> pore volume; <sup>c</sup> the initial heat of CO<sub>2</sub> adsorption; <sup>d</sup> Henry's Law selectivity at room temperature, <sup>e</sup> Langmuir surface area, <sup>f</sup> the data measured at this work.

**Table S3** Langmuir parameters for adsorption of CO<sub>2</sub>, CH<sub>4</sub>, and N<sub>2</sub> in **ZJNU-40a**.

	q <sub>sat</sub> (mol kg <sup>-1</sup> )	b <sub>0</sub> (Pa <sup>-1</sup> )	E (kJ mol <sup>-1</sup> )
CO <sub>2</sub>	17.8	2.05 × 10 <sup>-9</sup>	18.4
CH <sub>4</sub>	10.3	2.14 × 10 <sup>-9</sup>	15.4
N <sub>2</sub>	5	3.96 × 10 <sup>-9</sup>	13



**Table S4.** Langmuir parameters for adsorption of CO<sub>2</sub>, CH<sub>4</sub>, and N<sub>2</sub> in **NOTT-101**. The pure-component isotherm data for CO<sub>2</sub>, CH<sub>4</sub>, are from data measured in this work at temperatures of 273 K and 296 K. The pure-component isotherm data for N<sub>2</sub> are from Perry et al;<sup>22</sup> their data are reported at 273 K and 292 K.

	$q_{\text{sat}}$ (mol kg <sup>-1</sup> )	$b_0$ (Pa <sup>-1</sup> )	$E$ (kJ mol <sup>-1</sup> )
CO <sub>2</sub>	26	$1.24 \times 10^{-10}$	23.3
CH <sub>4</sub>	14	$1.04 \times 10^{-9}$	16
N <sub>2</sub>	5	$3.51 \times 10^{-9}$	13

## Notation

$b$	Langmuir constant for species $i$ at adsorption site A, Pa <sup>-1</sup>
$c_i$	molar concentration of species $i$ in gas mixture, mol m <sup>-3</sup>
$c_{i0}$	molar concentration of species $i$ in gas mixture at inlet to adsorber, mol m <sup>-3</sup>
$E$	energy parameter, J mol <sup>-1</sup>
$L$	length of packed bed adsorber, m
$p_i$	partial pressure of species $i$ in mixture, Pa
$p_t$	total system pressure, Pa
$q_i$	component molar loading of species $i$ , mol kg <sup>-1</sup>
$Q_{\text{st}}$	isosteric heat of adsorption, J mol <sup>-1</sup>
$t$	time, s
$T$	absolute temperature, K
$u$	superficial gas velocity in packed bed, m s <sup>-1</sup>

## Greek letters

$\varepsilon$	voidage of packed bed, dimensionless
$\tau$	time, dimensionless

## Reference

1. A. L. Myers and J. M. Prausnitz, *A.I.Ch.E.J.*, 1965, **11**, 121-127.
2. R. Krishna and J. R. Long, *J. Phys. Chem. C*, 2011, **115**, 12941-12950.
3. Y. He, R. Krishna and B. Chen, *Energy Environ. Sci.*, 2012, **5**, 9107-9120
4. E. D. Bloch, W. L. Queen, R. Krishna, J. M. Zadrozny, C. M. Brown and J. R. Long, *Science*, 2012, **335**, 1606-1610.
5. H. Wu, K. Yao, Y. Zhu, B. Li, Z. Shi, R. Krishna and J. Li, *J. Phys. Chem. C*, 2012, **116**, 16609-16618.
6. D.-L. Chen, H. Shang, W. Zhu and R. Krishna, *Chem. Eng. Sci.*, 2014, **117**, 407-415.
7. B. Zheng, H. Liu, Z. Wang, X. Yu, P. Yia and J. Bai, *CrystEngComm*, 2013, **15**, 3517-3520.
8. A. R. Millward and O. M. Yaghi, *J. Am. Chem. Soc.*, 2005, **127**, 17998-17999.
9. Y. He, S. Xiang, Z. Zhang, S. Xiong, C. Wu, W. Zhou, T. Yildirim, R. Krishna and B. Chen, *J. Mater. Chem. A*, 2013, **1**, 2543-2551.
10. Z. Liang, J. Du, L. Sun, J. Xu, Y. Mu, Y. Li, J. Yu and R. Xu, *Inorg. Chem.*, 2013, **52**, 10720-10722.
11. Y. Hu, S. Xiang, W. Zhang, Z. Zhang, L. Wang, J. Bai and B. Chen, *Chem. Commun.*, 2009, 7551-7553.
12. X. Duan, J. Yu, J. Cai, Y. He, C. Wu, W. Zhou, T. Yildirim, Z. Zhang, S. Xiang, M. O'Keeffe, B. Chen and G. Qian, *Chem. Commun.*, 2013, **49**, 2043-2045.
13. T. K. Prasad, D. H. Hong and M. P. Suh, *Chem. Eur. J.*, 2010, **16**, 14043-14050.
14. Z. Wang, B. Zheng, H. Liu, P. Yi, X. Li, X. Yu and R. Yun, *Dalton Trans.*, 2013, **42**, 11304-11311.
15. M. Zhang, Q. Wang, Z. Lu, H. Liu, W. Liu and J. Bai, *CrystEngComm*, 2014, **16**, 6287-6290.
16. Z. Wang, B. Zheng, H. Liu, X. Lin, X. Yu, P. Yi and R. Yun, *Cryst. Growth Des.*, 2013, **13**, 5001-5006.
17. N. H. Alsmail, M. Suyetin, Y. Yan, R. Cabot, C. P. Krap, J. Lü, T. L. Easun, E. Bichoutskaia, W. Lewis, A. J. Blake and M. Schröder, *Chem. Eur. J.*, 2014, **20**, 7317-7324.
18. R. D. Kennedy, V. Krungleviciute, D. J. Clingerman, J. E. Mondloch, Y. Peng, C. E. Wilmer, A. A. Sarjeant, R. Q. Snurr, J. T. Hupp, T. Yildirim, O. K. Farha and C. A. Mirkin, *Chem. Mater.*, 2013, **25**, 3539-3543.
19. X. Rao, J. Cai, J. Yu, Y. He, C. Wu, W. Zhou, T. Yildirim, B. Chen and G. Qian, *Chem. Commun.*, 2013, **49**, 6719-6721.
20. Y.-G. Lee, H. R. Moon, Y. E. Cheon and M. P. Suh, *Angew. Chem. Int. Ed.*, 2008, **47**, 7741-7745.
21. B. Zheng, R. Yun, J. Bai, Z. Lu, L. Du and Y. Li, *Inorg. Chem.*, 2013, **52**, 2823-2829.
22. J. J. P. IV, S. L. Teich-McGoldrick, S. T. Meek, J. A. Greathouse, M. Haranczyk and M. D. Allendorf, *J. Phys. Chem. C*, 2014, **118**, 11685-11698.